Passive Active L- and S-Band (PALS) Microwave Sensor for Ocean Salinity and Soil Moisture Measurements

William J. Wilson, *Fellow, IEEE*, Simon H. Yueh, *Member, IEEE*, Steven J. Dinardo, Seth L. Chazanoff, Ami Kitiyakara, Fuk K. Li, *Fellow, IEEE*, and Yahya Rahmat-Samii, *Fellow, IEEE*

***Abstract*—A passive/active L/S-band (PALS) microwave aircraft instrument to measure ocean salinity and soil moisture has been built and tested. Because the L-band brightness temperatures associated with salinity changes are expected to be small, it was necessary to build a very sensitive and stable system. This new instrument has dual-frequency, dual polarization radiometer and radar sensors. The antenna is a high beam efficiency conical horn. The PALS instrument was installed on the NCAR C-130 aircraft and soil moisture measurements were made in support of the Southern Great Plains 1999 experiment in Oklahoma from July 8–14, 1999. Data taken before and after a rainstorm showed significant changes in the brightness temperatures, polarization ratios and radar backscatter, as a function of soil moisture. Salinity measurement missions were flown on July 17–19, 1999, southeast of Norfolk, VA, over the Gulf Stream. The measurements indicated a clear and repeatable salinity signal during these three days, which was in good agreement with the Cape Hatteras ship salinity data. Data was also taken in the open ocean and a small decrease of 0.2 K was measured in the brightness temperature, which corresponded to the salinity increase of 0.4 psu measured by the M/V Oleander vessel.**

***Index Terms*—Radiometers, salinity, scatterometers, soil moisture.**

I. Introduction

MICROWAVE radiometry and scatterometry are well established techniques for surface remote sensing. Combining passive and active sensors provides complementary information contained in the surface emissivity and backscatter signatures, which may improve the accuracy in the retrieval of geophysical parameters. For example, over the ocean, the low-frequency passive radiometer brightness temperature is a function of the sea surface temperature (SST), the sea surface salinity (SSS), the surface roughness from wind and waves, and the atmospheric emission (at L- and S-bands, it is possible to accurately model the atmospheric emission and correct the data). Using dual frequencies and dual polarization provides information on the SST, SSS, and roughness. However, it has been shown that by adding an active scatterometer, more information on the surface roughness is provided, which will significantly improve the accuracy of the retrieved SSS [1]. Over land, it has been demonstrated that the radiometer and the scatterometer both provide information for estimating soil moisture and vegetation biomass [2].

To investigate the benefits of combining passive and active microwave sensors, the Jet Propulsion Laboratory (JPL), with NASA support, has designed, built, and tested a new precision passive/active L/S-band (PALS) microwave aircraft instrument for measurements of ocean salinity and soil moisture. Because the L-band brightness temperature variations associated with salinity changes are small, it was necessary to build a very accurate, sensitive, and stable system. (At a SST of 28 °C a salinity change of 0.2 psu results in a brightness temperature change of 0.15 K, and at 10 °C only 0.08 K.) After a series of simulations of radiometer and radar measurements [3], the instrument requirements were determined to allow salinity measurements to be made with an accuracy of 0.2 psu over the open ocean. This new instrument has dual-frequency (L- and S-band), dual polarization radiometer and polarimetric radar sensors and was installed in the National Center for Atmospheric Research (NCAR) C-130 aircraft. The antenna is a high beam efficiency conical horn with relatively low sidelobes pointed at a 38° incidence angle to the ocean surface. An IR temperature sensor was used to measure the changes in the sea surface temperature. To achieve maximum radiometer stability a three position Dicke switching scheme was used with a noise diode calibration. The radar electronics calibration was achieved using an internal calibration loop.

II. System Description

An overall block diagram of the PALS instrument is shown in Fig. 1, and the key system characteristics are summarized in Table I. The design challenges in this system were getting a high beam efficiency low-frequency antenna system with a small footprint, and in developing a stable, well-calibrated aircraft radiometer and radar system. Details on each of the subsystems are presented below.

A. Antenna

A number of antenna designs were considered for this precision L/S-band instrument. The basic requirements were to achieve

Manuscript received April 4, 2000; revised November 27, 2000. This work represents one phase of research carried out at the Jet Propulsion Laboratory, California Institute of Technology, under contract with the National Aeronautic Space Administration. This work was supported by the NASA Code Y Earth Science Enterprise Office, Ocean Science Program.

W. J. Wilson, S. H. Yueh, S. J. Dinardo, S. Chazanoff, A. Kitiyakara, and F. K. Li are with the Jet Propulsion Laboratory, California Institute of Technology, Pasadena, CA 91109 USA (e-mail: william.j.wilson@jpl.nasa.gov).

Y. Rahmat-Samii is with the Department of Electrical Engineering, University of California, Los Angeles, CA 90094 USA (e-mail: rahmat@ee.ucla.edu).

Publisher Item Identifier S 0196-2892(01)03826-8.

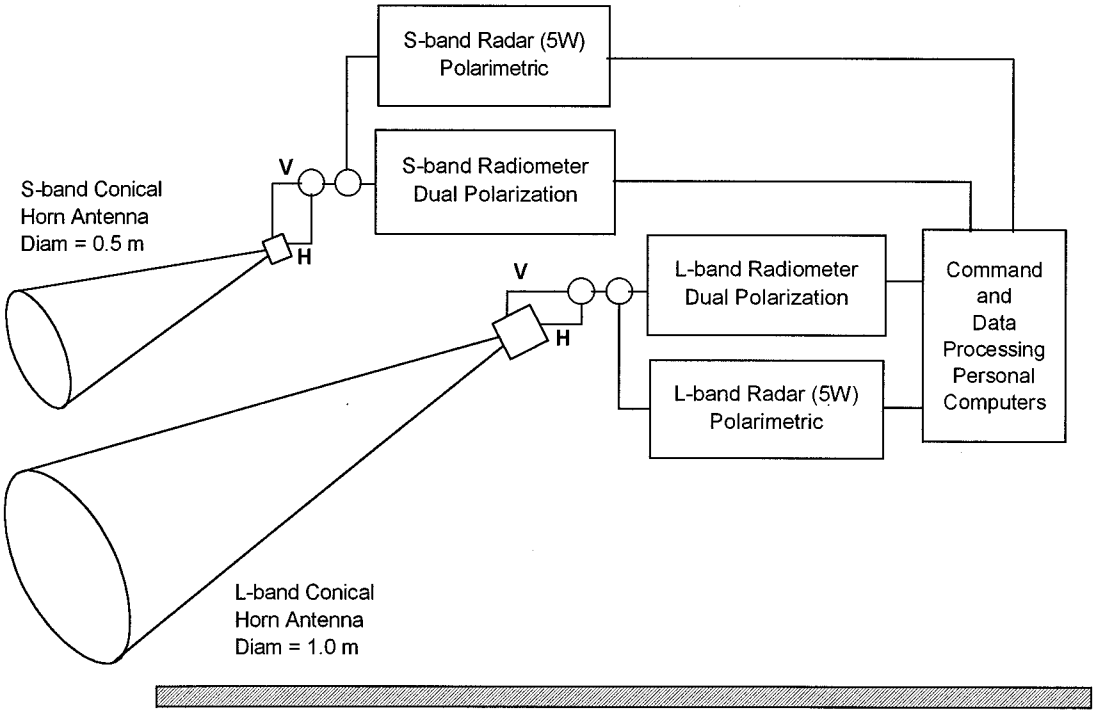

Fig. 1. PALS overall system block diagram showing the separate L and S-band radiometers and radars.

TABLE I
PALS SYSTEM CHARACTERISTICS

Radiometer Frequencies (L & S)	1.41 and 2.69 GHz
Radiometer Polarizations	Vertical (V) and Horizontal (H)
Radar Center Frequencies (L & S)	1.26 and 3.15 GHz
Radar Polarizations	VV, HH, VH
Antenna Type	Conical Horns
Aperture Diameters (L & S)	1.0 and 0.5 m
Antenna Gain and Beam Efficiency	23 dB and > 92%
Antenna Beam Incidence Angle	38°
Antenna Footprint Spatial Resolution at 1.2 km altitude	0.6 km
Radiometer Bandwidth (L & S)	20 and 5 MHz
Radiometer NEDT per Footprint (L & S)	0.12 and 0.28 K
Radiometer Absolute Accuracy	± 2 K
Radar Transmit Power and Duty Cycle	5 Watts and 8%
Radar Noise Equivalent σ_o at 1.2 km altitude	< -45 dB
Radar Calibration Stability	0.1 dB

low loss, beam efficiencies >90% sidelobes <20 dB, and cross polarization isolation >20 dB. Additionally, the antenna was to be low cost and built in a short time. It was concluded that with these constraints, the best choice for the antenna to meet these requirements was the conical horn. (It should be noted that at L-band, an offset parabolic reflector antenna with a 1-m diameter would have a feed horn nearly as large as the conical horn used, and would be more difficult to accommodate on the aircraft.) The two conical antenna horns were made with 0.125-in thick rolled sheet aluminum, with the conical sections riveted together. The L-band antenna has an output diameter of 1.0 m and a length of 2.7 m. The S-band antenna has an output diameter of 0.5 m and a length of 1.7 m.

A waveguide to coax orthomode transducer (OMT) is attached to the end of the horn to separate the Vertical (V) and Horizontal (H) polarizations. The calculated and measured antenna patterns of the S-band horn are shown in Fig. 2. This data shows the good agreement between the calculated and measured antenna patterns. (The difference between the measured and calculated cross-polarized patterns at 0° is probably due to a small misalignment in the antenna range mounting fixture.) These characteristics of the S-band antenna are summarized in Table II. The L-band antenna pattern was not measured because of time and budget restrictions. However, because the L-band antenna was a scaled copy of the S-band antenna, the calculated parameters for the L-band antenna horn were judged to be adequate for the system calibrations in this paper. It is planned to measure the L-band antenna pattern in the near future, so a more accurate data analysis can be made.

At each frequency, the conical horn antenna is time shared between the radiometer and radar. The system is switched to the radar scatterometer 17% of the time. The system is also switched between the two polarizations so that only one set of radar and radiometer electronics was required for each frequency band. This feature also improved the relative calibration accuracy between the two polarizations; however, it reduced the data integration time, which was not a problem in this slow moving, single beam aircraft system.

The two antenna horns were mounted in an aluminum frame and installed on the back ramp of the C-130 aircraft. During the flights, the ramp of the C-130 aircraft was lowered and the frame assembly was raised to the position where the antennas were pointing down to the 38° incidence angle. A photograph of the raised antenna assembly is shown in Fig. 3. (The antenna angle with respect to the C-130 ramp vertical angle was 40°. With the nominal aircraft pitch angle of ~2° during the flights, this

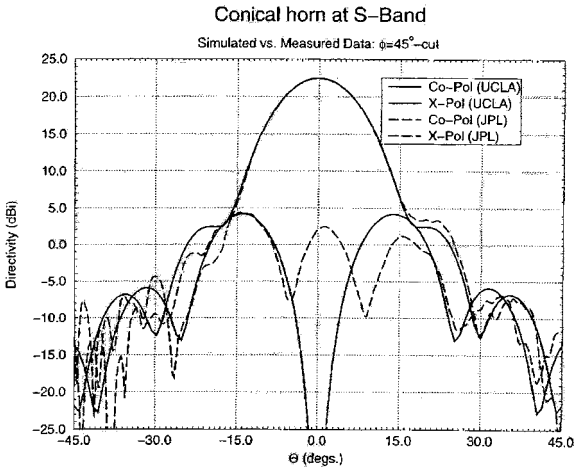

Fig. 2. S-band calculated and measured antenna patterns in 45° plane for the conical horn. Both copolarized and cross-polarized patterns are shown. Due to imperfections in the horn construction and/or small antenna range alignment errors, the measured cross-polarization pattern did not show the deep null of the calculated pattern at 0°.

TABLE II
S-BAND ANTENNA CHARACTERISTICS IN A 45° PLANE

Parameter	Calculated	Measured
3 dB Beamwidth (HPBW)	13.4°	13.2° ± 0.3°
Beam Efficiency (Power in 2.5*HPBW over ± 45°)	92.7%	93.3% ± 1%
Gain	+23 dB	not measured
1st Sidelobe level	-21 dB	-20 dB ± 1 dB
Cross Polarization Isolation	-19 dB	-20 dB ± 1 dB

put the incidence angle at 38° on the surface. In future flights, this angle can be adjusted to a value between 35° and 55°, if desired.)

B. Radiometer

In the design of the precision radiometer, it was decided to use a noise diode injection scheme, along with a three sequence Dicke switching cycle as described in Section III. All components following the antennas are mounted in temperature controlled boxes which were stable to ±0.1 °C. In the block diagram shown in Fig. 4, the noise diode calibration signal is injected into the radiometer immediately following the OMT to calibrate gain variations in all the following stages.

In this design, there are two PIN diode switches to switch between antenna polarizations and the radar. The 3-pole polarization switch is also used as the Dicke switch to switch to the internal reference load. A 75 MHz bandpass filter is used for radio frequency interference (RFI) rejection in the input to the low noise amplifier (LNA) at both L-band and S-band.

The front end radiometer signals are sent via coax cable to the radiometer back end located in the PALS control rack in the forward part of the aircraft. Here the signal is put through another bandpass filter, amplified and then mixed down to a 200 MHz center intermediate frequency (IF). The main reason for this frequency conversion was to allow tuning the radiometer over the front end bandwidth with a narrowband IF to avoid RFI during the measurements. During the measurements, both in Oklahoma and Virginia, it was found that a 20-MHz bandwidth IF filter was usually adequate for the L-band radiometer to avoid the RFI. However, it was necessary to use a 5-MHz bandpass IF filter in the 2.7-GHz S-band, to get an acceptable signal. Even then, there were times that the RFI contaminated the S-band data because it was broadband interference.

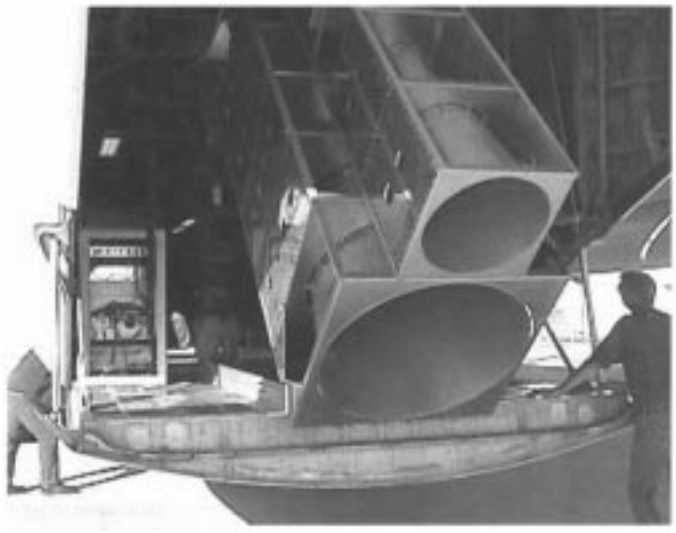

Fig. 3. Photograph of the L and S-band horn antennas on the rear ramp of the C-130 aircraft raised to the observing position.

Following the IF amplifier, the signal was square-law detected using a tunnel diode detector and the detected output sent to the analog integrator circuit. After the 350 μs integration time, the analog signal was converted to a digital signal for the radiometer computer with a 12-bit A/D converter. One design note to mention is that was necessary to use a Teflon capacitor in the integrator circuit, to reduce the effect of dielectric absorption, because the integrator dump time is only 50 μs. Because of the relatively slow velocity of the C-130 aircraft of 0.07 km/s (140 kn), the effective radiometer integration time is $\sim$4 s for each polarization for each footprint.

C. Radar

The dual frequency radar system is a pulse radar system with a 2.86 kHz pulse repetition frequency (PRF) and an output power of 5 W. The radar block diagram is shown in Fig. 4. During the radar operation, a 27 μs pulse is transmitted in Vertical (V) polarization, and then the front end switches are set to receive the return V pulse. For the next pulse, 350 μs later, a Horizontally (H) polarized pulse is transmitted and then received. The third pulse transmitted is in V, and then the cross polarized H pulse, is received. For the next series of three pulses, the frequency is changed by 2 MHz to get an independent sample, and the cycle is repeated. There is a series of 10 "frequency hops" over a 20-MHz bandwidth, in a complete cycle, before it repeats. This separates the same polarization and frequency radar pulses by 10 ms, or by a distance of $\sim$ 0.7 m, which is more than one half the antenna aperture, to insure that the radar samples are independent.

The radar front end is located near the antenna horns to keep the input losses down. A preselection filter is used before the LNA to reduce the RFI. The amplified received signal is sent

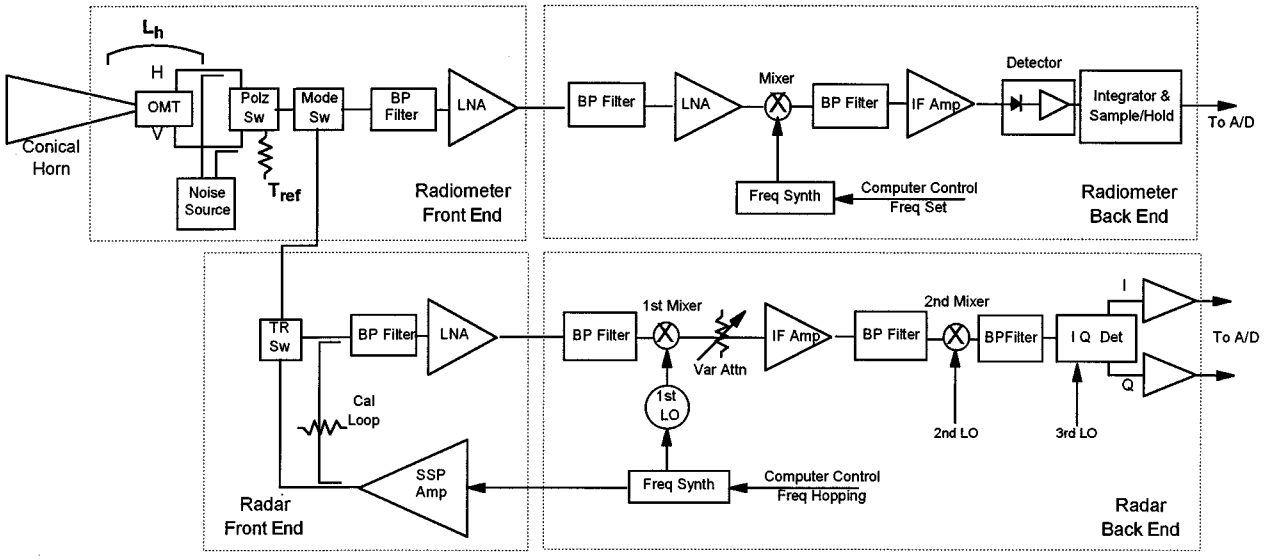

Fig. 4. PALS system block diagram of radiometer and radar electronics. Only one frequency channel is shown. The radiometer and radar front ends are located near the antenna horns, and the back ends are located in the forward part of the aircraft.

back to the radar back end electronics located in the operator's control rack. The received signal is mixed down to an IF of 400 MHz, where it is filtered with a 10 MHz wide bandpass filter. At this point, the 1st LO is in synchronization with the transmitter frequency hopping, and thus the IF signal is a constant 400 MHz. After amplification, this signal is mixed down to 70 MHz and sent through the I/Q detector to measure the in-phase and quadrature-phase components of the received signal. The I/Q signals are filtered to a 1 MHz bandwidth, and then sampled with a 12-bit A/D converter at a rate of 2 MHz, during the range gate. This results in about 20 samples of the received pulse, which are used to calculate the average power of HH, VV, VH, and their mutual correlations $\langle \mathrm{HHVV}^* \rangle$, $\langle \mathrm{HHVH}^* \rangle$, and $\langle \mathrm{VVVH}^* \rangle$. It should be noted that all the radar local oscillator (LO) signals are phase locked to a 10-MHz reference oscillator to provide phase coherence among all the signals. Also, all the electronics boxes are temperature controlled with a stability of ± 0.1 °C.

D. Control and Data

The control and data system for PALS uses three Pentium II based personal computers, networked together, as shown in Fig. 5. The timing and radar control software was written in the Microsoft Visual C++ language operating with the Windows 95 Rev 2 operating system. The radiometer control software was written in Microsoft Visual Basic 5.0, also operating with Windows 95 Rev 2.

The timing computer is used to generate all the system timing signals, using a high-speed digital interface card. This provides all the signals for the radar and the radiometer to switch between the different operating modes and for the data conversion and collection. The advantage of this approach is that it is relatively straightforward to program the timing signals, and it was fast to change signals as the system design evolved.

The radar computer controls the IF attenuator and processes and records the radar data. The radar data, which includes the I, I^2, Q, and Q^2, and mutual correlations, are averaged into 0.5-s intervals and written to the hard disk. The radar computer also takes input commands from the operator and provides a real time data display. The radiometer computer controls the LO frequency, reads in the radiometer data, averages it into 0.5-s samples, writes it to its hard disk, and provides a real time data display. The radiometer computer also records the physical temperatures of the horns and electronics every minute. Following each data flight, all the data is backed up on both floppy disks and a CD-ROM.

The aircraft engineering data, which includes the aircraft location, altitude, attitude, heading, and IR temperature sensor, was transmitted to both the radiometer and radar computers at 1-s intervals by the NCAR C-130 data system. This data was incorporated directly in the radiometer and radar data files.

III. Calibration

A. Radiometer

The PALS radiometers are calibrated with a noise diode source that is injected following the antenna horn and OMT. A three-sequence switching cycle is used for the observations to achieve maximum stability. In this scheme, the radiometer is alternately switched between the antenna, the antenna plus noise, and the reference load. The Dicke switching rate was $\sim$ 80 Hz, to effectively eliminate any system gain variations.

The radiometer antenna temperatures T_{a} are calculated using the following equation:

$$T_{\mathrm{a}} = T_{\mathrm{h}} + L_{\mathrm{h}}^{*}\left[T_{\mathrm{ref}} - T_{\mathrm{h}} - T_{\mathrm{nd}}^{*}\frac{(V_{\mathrm{r}} - V_{\mathrm{a}})}{(V_{\mathrm{n}} - V_{\mathrm{a}})}\right] \tag{1}$$

where

T_{h} temperature of the antenna input loss L_{h};
L_{h} antenna horn, OMT, and input cable loss;
T_{ref} temperature of the reference load;
T_{nd} effective temperature of the noise diode source;
V_{r} output voltage when switched to the reference load;
V_{a} output voltage when switched to the antenna;

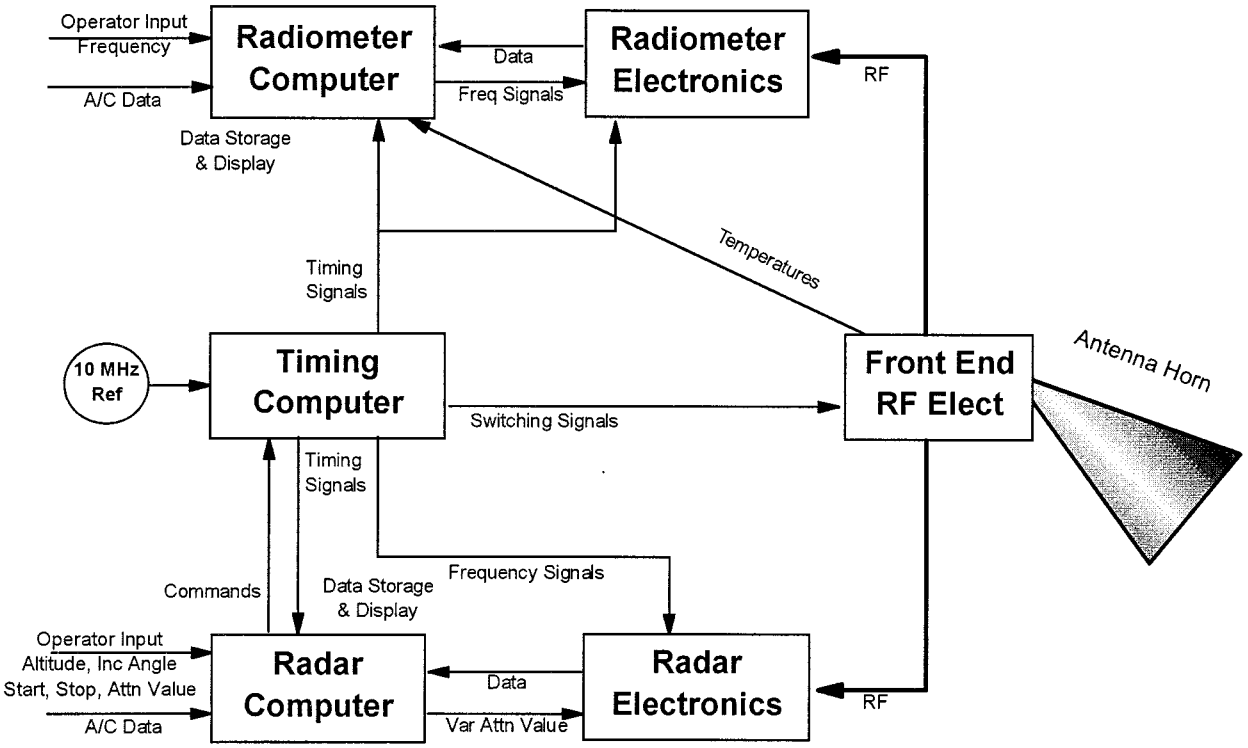

Fig. 5. PALS control and data system block diagram showing the three personal computers and their connections and functions.

$V_{\rm n}$ output voltage when switched to the antenna with the noise source on.

As seen from (1), the advantage of this three position Dicke switching scheme, is that the measured antenna temperature depends on very stable quantities. However, it should be noted that (1) contains the input loss term $L_{\rm h}$, which is difficult to measure. (It was assumed that most of this loss was in the horn throat, the OMT and the input cable to the noise diode coupler. The temperature of this loss was assumed to be the average of the horn throat, OMT and baseplate temperatures.) The approach that was taken with the PALS radiometer was to make observations of a known source, which we could accurately predict the antenna temperature, and then calculate the value of $L_{\rm h}$ to match the measured and predicted temperatures.

On July 11, the absolute calibration of the radiometers was made by measuring the antenna temperatures while flying at 300-m altitude over a fresh water lake in Oklahoma with a nominal incidence angle of 38°. The incidence angle of the measured antenna temperatures was corrected for the roll and pitch of the aircraft with an accuracy of 0.1° every second. The corrected antenna temperatures were then compared to the calculated temperatures from a model using the dielectric constant of fresh and sea water given by Klein and Swift [4]. The temperature of the lake was measured from the aircraft using an IR sensor to be 28 °C, and the wind speed was estimated from visual observations to be 3–5 m/s. These parameters were included in the model and the predicted antenna temperatures were calculated to be $T_{\rm a}V = 137.8$ K and $T_{\rm a}H = 97.2$ K for L-band and S-band. A wind velocity sensitivity of 0.3 K per m/s was used based on Hollinger [5] and Swift [6] measurements and our ocean measurements over buoys. Note that these values include the reflected atmospheric and cosmic background emission (∼3.4 K at V and ∼ 4.2 K at H) and the *in-situ* atmospheric emission of ∼0.5 K. Following the flight on July 11, the noise diode source was calibrated using ambient and liquid nitrogen cooled coax loads connected to the radiometer inputs at the OMT/antenna horn. From these data, it was possible to calculate the input loss values for $L_{\rm h}$ for both frequencies and polarizations. These values were L-band: $L_{\rm hV} = 1.14\ (0.57\ {\rm dB})$, $L_{\rm hH} = 1.15\ (0.61\ {\rm dB})$, S-band: $L_{\rm hV} = 1.09\ (0.37\ {\rm dB})$, and $L_{\rm hH} = 1.08\ (0.33\ {\rm dB})$.

On other measurement days in Oklahoma, these loss values were used, and the temperature of the noise diode was adjusted to bring the measured lake brightness temperatures into agreement with the model calculations. Only *small* changes in $T_{\rm nd}$ were necessary from day to day, which were due to changes in the front end cables from system troubleshooting. Absolute calibrations using models may have absolute errors of 1–2 K; however, the relative day to day errors should be <1 K.

During the Atlantic Ocean measurements on July 17–19, passes were made over the NDBC Buoy 41 001 in a star pattern at an altitude of 1250 m. The passes, which did not have apparent sun glint, were chosen for the calibration runs. For this case, the model was run with an SSS $= 36$ psu, using the temperature of 28 °C, and a wind speed of 5 m/s. (The temperature and wind speed were taken from the buoy data, which were constant over the measurement time, and the value of 36 psu was used based on data from the Cape Hatteras ship.) The predicted temperatures for an incidence angle of 38° were: $T_{\rm a}V = 116.4$ K, $T_{\rm a}H = 81.2$ K for L-band, and $T_{\rm a}V = 130.6$ K, $T_{\rm a}H = 91.7$ K for S-band. (Note that these

values also include the reflected atmospheric and cosmic background emission and the *in-situ* atmospheric emission for a total of ~ 5 K.) Using the July 11 loss values, the noise diode value was calculated to match the predicted ocean temperatures. During *all* the July Ocean measurements, the noise source temperature was set to this value. Based on this calibration procedure, it is estimated that the absolute calibration of the radiometers for this set of measurements was within ± 2 K.

B. Radar

The radar signal is calibrated by measuring a small fraction of the transmitted power$(-90$ dB$)$, and receiver gain through the calibration loop and receiver, and then using the measured system losses, antenna gain, and target range to calculate the radar target cross section, σ_{o}. During the normal data taking, the received signal is measured with the range gate adjusted to receive the return pulse and the IF attenuator set to the data value. During the short calibration cycle, every 10 s, the signal is measured during the transmit time with the IF attenuator set to a higher calibration value. Following this measurement, the transmitter is turned off and the system noise signal is measured with the IF attenuator set at the calibration value and then the data value.

In terms of the absolute value, the measured antenna gain and the receive and transmit losses, were used for the radar calibration, and it is estimated that the values of σ_{o} have errors ± 2 dB. With the calibration loop, the radar calibration depends on stable quantities, and the relative measurements over periods of a few hours are expected to be within 0.1 dB.

IV. Test Flights

Under an agreement with the National Science Foundation, the PALS instrument was installed on the NCAR C-130 aircraft in May/June 1999. Because of the large size of the antenna horns, this was the most practical aircraft for the PALS instrument. The instrument was mounted with the antenna assembly installed on the rear ramp of the aircraft, which was closed during takeoff and landing. When up to the cruising altitude of $\sim$1.3 km (3900 ft), the ramp was lowered, and the antenna assembly was raised to have the antennas pointing down at a 38° incidence angle. In July 1999, the PALS instrument was used for two missions — soil moisture and ocean salinity.

A. Soil Moisture

The first mission was making measurements of soil moisture in the Little Washita Watershed near Oklahoma City from July 8 to 14. This was in support of the Southern Great Plains 1999 experiment (SGP99). Six flights were made during this period. It rained on July 10th, so it was possible to get dry data on July 8 and 9, and then monitor the drying out from July 11 through July 14. Samples of the L-band radiometer and radar data from July 9 and July 11, on line 9E are shown in Fig. 6. (The S-band data has a similar shape with slightly less polarization difference.) The surface IR temperature was $31.8°\mathrm{C} \pm 1°\mathrm{C}$ on July 9, and $23.0° \pm 1.5°\mathrm{C}$ on July 11 over this line.

The western part of this line had less vegetation and received greater precipitation, which accounts for the larger brightness temperature variations of 40–50 K before and after the rainstorm. This also explains the larger radar backscatter difference of 2–5 dB on the wetter July 11. The changes in the radar backscatter are much larger than the changes in the brightness temperature, which is consistent to the greater radar sensitivity to surface roughness and vegetation. This set of soil moisture data has been analyzed, and a paper has been presented [7].

B. Ocean Salinity

Three flights were made for ocean salinity measurements. These were on July 17–19, 1999, southeast of Norfolk VA, over the Gulf Stream, and out into the open ocean. The surface truth measurements of SSS, SST, and surface winds were gathered by Stephan Howden from the Goddard Space Flight Center (GSFC) on the Cape Hatteras ship from Duke University. The L-band radiometer and radar data from flights on July 18 over the Gulf Stream along with the ship data are shown in Fig. 7. These data show that the L-band brightness temperature decreased about 3 K in both polarizations when crossing the Gulf Stream. Along this line, the ship data shows an increase of 5 psu in the ocean salinity. The aircraft line and the ship line were separated by $\sim$ 20 km, which may account for the slight differences in the alignment of the salinity and brightness temperature gradients. The change in the S-band brightness temperature was $\sim$1 K, which indicates a decrease in SSS sensitivity at the higher frequency. Note that the radar data shows relatively small changes in the surface roughness due to wind, and this roughness effect was corrected in the radiometer data (an empirical correction of $-300^{*}\sigma_{\mathrm{oLH}}$ was used on the radiometer data. This factor was based on area where the wind velocity changed for 0 to 5 m/s.) This data has also been corrected for the changes in the SST assuming a change of 0.2 K per 1 °C in SST. There also may be a small correction for wind direction; however, this dependence is not known at this time. The area of surface roughness correction will be a major area of future PALS research.

To show the ability of the PALS system to measure small salinity changes, part of the flight path on July 18 covered the path of the M/V Oleander vessel, which had transited the day before. The M/V Oleander is a container cargo ship, which has a NOAA salinity sensor and measures the salinity on its route between Port Elizabeth, NJ and Hamilton, Bermuda, every week. The radiometer and radar data over the M/V Oleander path is shown in Fig. 8, along with the salinity data provided by the M/V Oleander. This shows an L-band brightness temperature decrease of $\sim$0.2 K. (This value has been corrected by 0.1 K due to the IR temperature increase of 0.5 K.) In this line, the radar backscatter was nearly constant, and thus only small corrections to the radiometer data for surface roughness were required. Over this path, the salinity data measured the day before increased by 0.4 psu, which is consistent with the decrease in the measured brightness temperature.

To show the stability of the system during the ocean measurements, two sets of data taken on July 19, separated by two hours over the same area, were compared. These data showed the average $(\mathrm{Vertical}+\mathrm{Horizontal})$ brightness temperatures over this area were within 0.2 K for these two sets of data, which confirms the estimate of system stability.

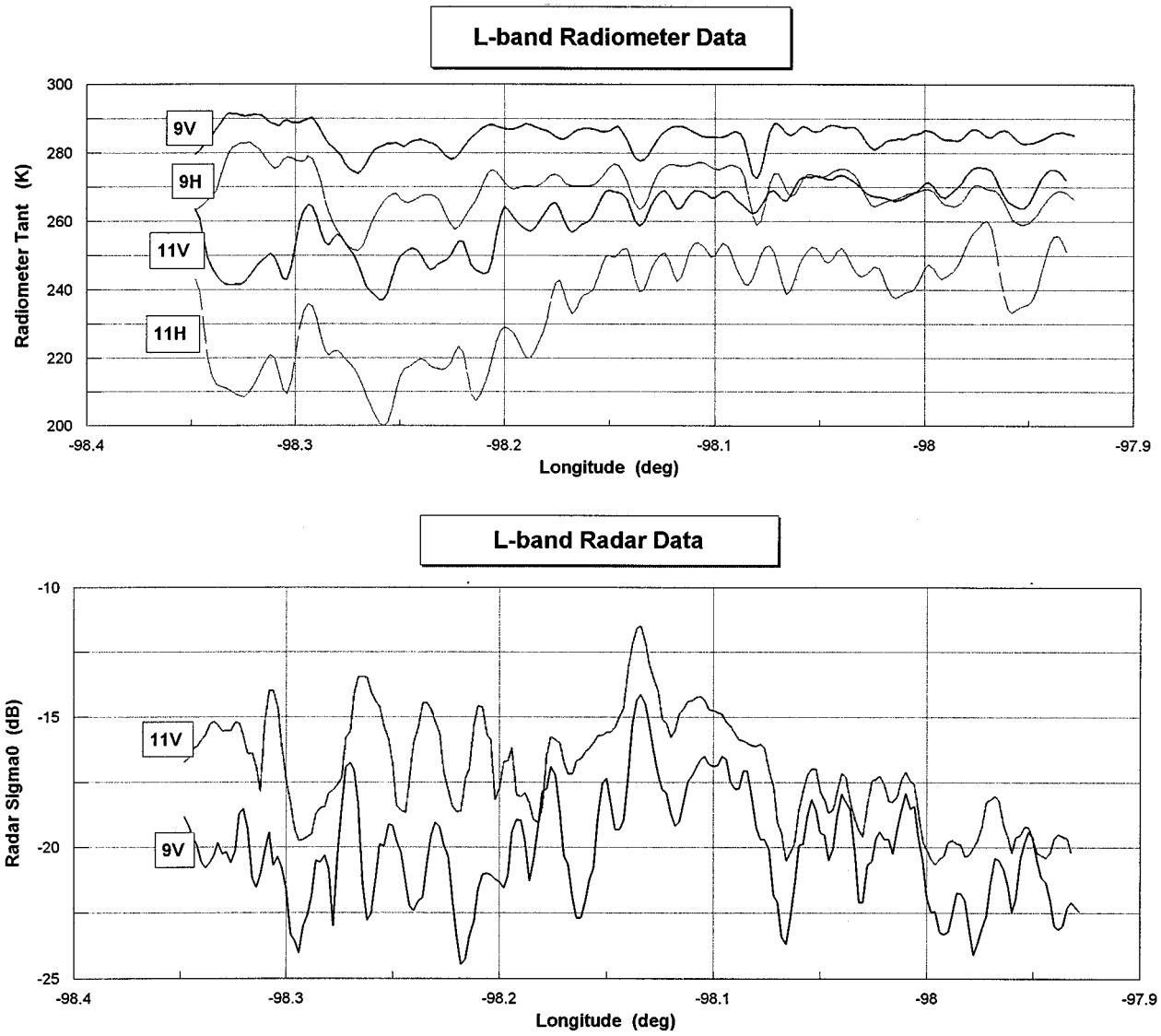

Fig. 6. Soil moisture data from line 9E on July 9 and 11 at ~10 am in the Little Washita Watershed before and after a rainstorm which occurred on July 10. The latitude was 34.935°. The notation refers to the date and polarization. Only the vertical polarization is shown in the radar data to reduce the confusion of overlapping plots. (The notation 9V and 11V indicate the VV $\sigma_\circ$ from July 9 and 11, respectively.) Note the large decrease in the radiometer brightness temperatures of ~10-50 K, and the increase of ~2-5 dB in the radar cross section with the wetter conditions on July 11.

V. Summary

A passive/active L/S-band (PALS) microwave aircraft instrument has been built and tested. The purpose of this instrument was to make precision remote sensing measurements for the development of improved algorithms for retrieval of soil moisture and ocean salinity. In July 1999, the instrument was used in Oklahoma in support of the SGP99 experiment. Also in July 1999, the instrument was used off the coast of Virginia and North Carolina to measure the ocean brightness temperatures to develop models for ocean salinity retrievals. The measurements were successful, and the detailed science results will be published shortly. The measurements demonstrated a radiometer with an absolute accuracy < 2 K, with a relative stability of ~0.2 K over a few hours. The radar also showed an absolute accuracy of ± 2 dB, and a stability of 0.1 dB over a few hours.

There are two factors on the ocean measurements that deserve comment. One constant problem with the ocean measurements near Norfolk, VA, was the nearly constant RFI at the S-band frequency. The RFI was very broadband and usually contaminated the S-band signal by 0–5 K. This was disappointing; however, on Sunday, July 18, the RFI was noticeably less and many of the S-band measurements were of good quality.

The other aspect of the ocean measurements was the effect of the sun's reflection, or sun glint, into the antenna sidelobes. At L-band the sun is a very strong source with an effective temperature $> 100\,000$ K, and this can be a major source of interference for antennas with high sidelobes. The advantage of the PALS conical horn antennas, with their relatively low sidelobes, and observing from the rear of the C-130 aircraft, was that if the reflected sun image was $> 45°$ from the antenna beam direction, there was no detectable interference. Most important observations were scheduled near local noontime to reduce the effect of sun glint. However, when the data showed possible sun interference, it was always possible to reverse the flight direction

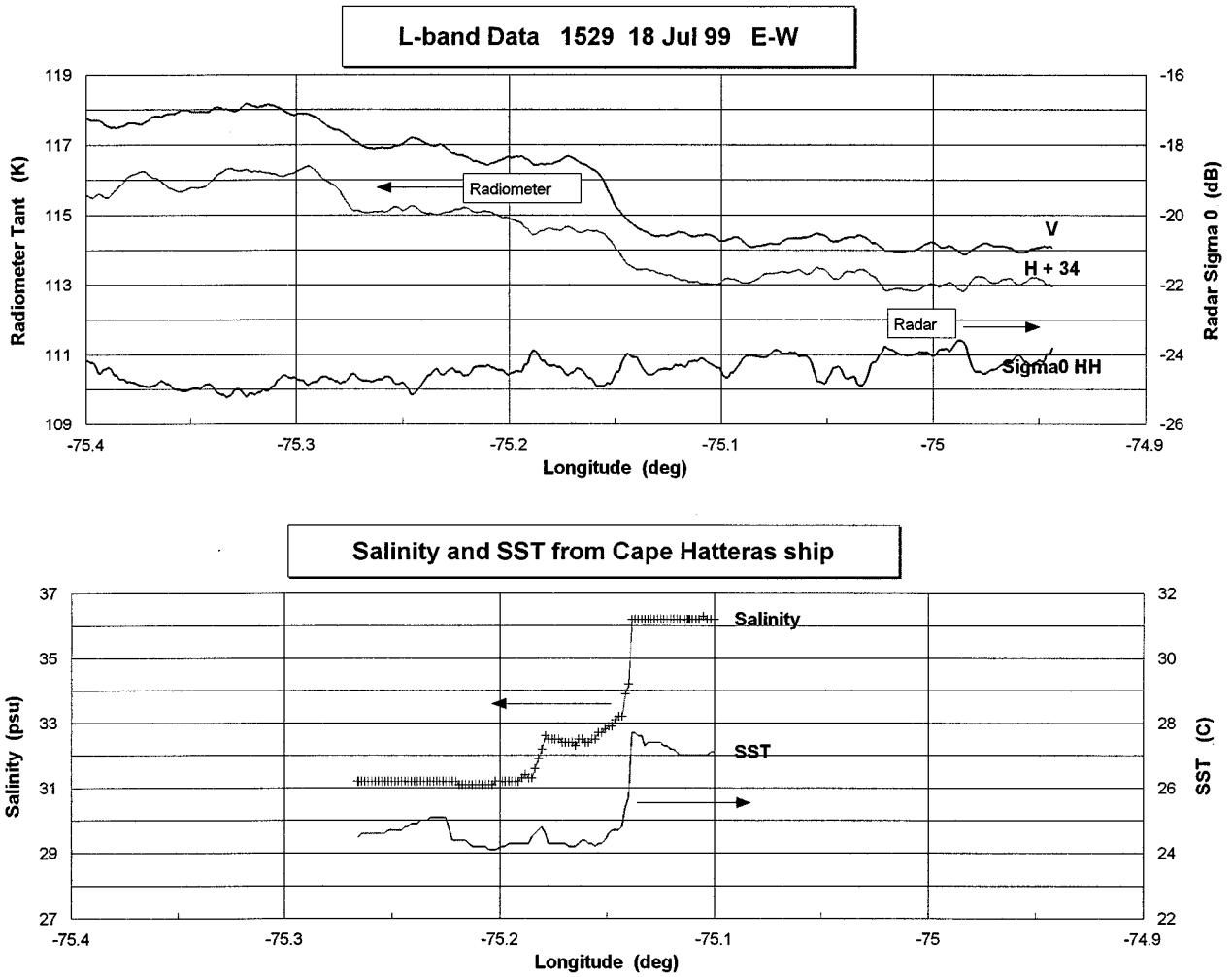

Fig. 7. L-band brightness temperature and ocean salinity data over the Gulf Stream on July 18, 1999. Corrections to the radiometer data have been made for surface roughness and surface temperature changes. The H polarization radiometer data is offset by +34 K to show both sets of data on the same plot. The average latitude of the aircraft was 35.51° and the average latitude of the ship was 35.31°. The increase in the brightness temperatures, corresponding to the decrease in the salinity, is not aligned exactly due to the slight difference in the position of the measurements.

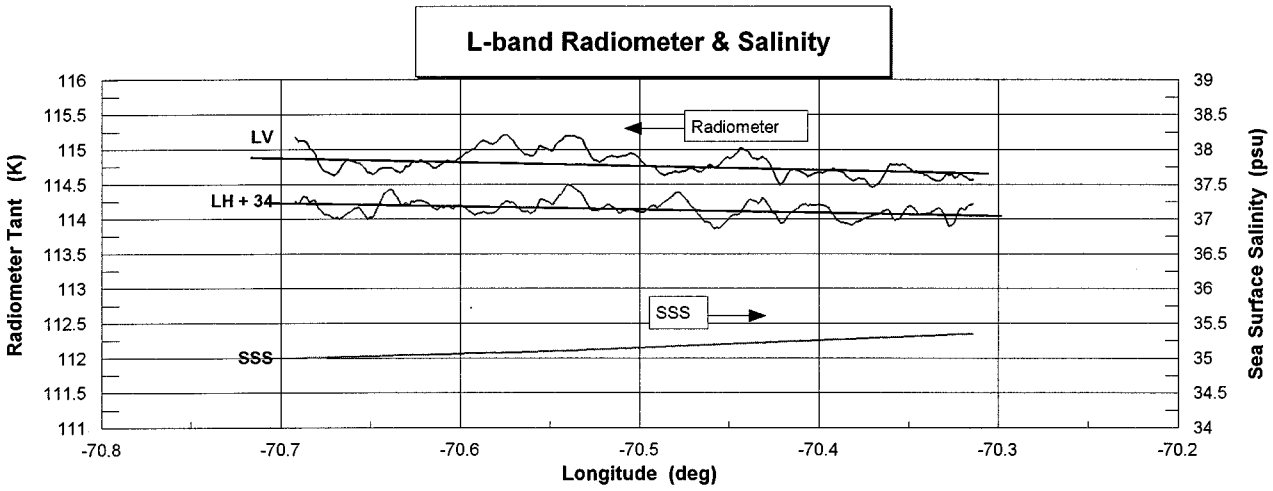

Fig. 8. Open ocean salinity data along the line of the M/V Oleander on July 18, 1999. The horizontal L-band data has a +34 K bias to show both curves on the same scale. Both polarizations of the L-band radiometer data are shown with a linear curve fit. The SSS are data from the M/V Oleander thermo salinograph (TSG) on July 17, 1999.

to eliminate the effect. Future measurements will be planned during the night to completely avoid this problem.

It is planned to improve the calibration accuracy and stability of the PALS radiometers, by adding mechanical switches just

after the antenna to allow switching in ambient and cooled loads periodically during the flight measurements. This will serve to accurately calibrate the noise diode and any temperature offsets. At the low frequency of L-band, it is not practical to place the large ambient and cold loads in front of the antenna. This approach to make absolute system calibrations, just after the antenna, using calibrated and stable coaxial loads, and then using known water targets to calibrate the antenna losses, will significantly improve the absolute calibration and the day to day stability. Plans for future PALS instrument experiments include additional open ocean measurements of the SSS and support for soil moisture measurement campaigns.

ACKNOWLEDGMENT

The authors would like to thank the crew of the NCAR C-130 aircraft for their support and help during these missions. They also thank S. Howden and the crew of the Cape Hatteras for their help during the salinity missions. They also thank R. Hoferer of UCLA for his assistance in computing the horn patterns.

REFERENCES

[1] S. H. Yueh, R. West, W. J. Wilson, F. K. Li, E. G. Njoku, and Y. Rahnat-Samii, "Error sources and feasibility for microwave remote sensing of ocean surface salinity," *IEEE Trans. Geosci. Remote Sensing*, vol. 39, pp. 1049–1060, May 2001.

[2] J.-P. Wigneron, P. Ferrazzoli, J.-C. Calvet, Y. Kerr, and P. Bertuzzi, "A parametric study on passive and active microwave observations over a soybean crop," *IEEE Trans. Geosci. Remote Sensing*, vol. 37, pp. 2728–2733, Nov. 1999.

[3] E. G. Njoku, W. J. Wilson, S. H. Yueh, and Y. Rahmat-Samii, "A large-antenna microwave radiometer-scatterometer concept for ocean salinity and soil moisture sensing," *IEEE Trans. Geosci. Remote Sensing*, vol. 38, pp. 2645–2655, Nov. 2000.

[4] L. A. Klein and C. T. Swift, "An improved model for the dielectric constant of sea water at microwave frequencies," *IEEE Trans. Antennas Propagat.*, vol. AP-25, pp. 104–111, Jan. 1977.

[5] J. P. Hollinger, "Passive microwave measurements of sea surface roughness," *IEEE Trans. Geosci. Electron.*, vol. GE-9, pp. 165–169, July 1971.

[6] C. T. Swift, "Microwave radiometer measurements of the Cape Cod Canal," *Radio Sci.*, vol. 9, no. 7, pp. 641–653, 1974.

[7] E. G. Njoku, W. J. Wilson, S. H. Yueh, T. Jackson, V. Lakshmi, and J. Bolter, "Soil moisture and vegetation observations during SGP99 using the POLS airborne radiometer-radar system," *IEEE Trans. Geosci. Remote Sensing*, to be published.

William J. Wilson (S'59–M'64–SM'86–F'98) received the B.S.E.E. degree from the University of Washington, Seattle, in 1961, and the M.S.E.E., E.E., and Ph.D. degrees in electrical engineering from the Massachusetts Institute of Technology, Cambridge, in 1963, 1964, and 1970, respectively.

In 1964, he served in the U.S. Air Force, working on military communication satellites. In 1970, he joined the Aerospace Corporation, Los Angeles, CA, and was involved in the design and construction of the millimeter-wave receivers and radio astronomy observations. In 1976 and 1977, he was an Assistant Professor in the Electrical Engineering Department, University of Texas, Austin. He returned to the Aerospace Corporation in 1977, where he was involved with research in millimeter-wave radiometers and low-noise receivers. In 1980, he joined the staff of NASA's Jet Propulsion Laboratory (JPL), Pasadena, CA, where he is the Supervisor of the Microwave Advanced Systems Group. At JPL, he has been working on low-noise microwave and millimeter-wave radiometers and radar systems for aircraft and spacecraft for Earth remote sensing applications. He is currently a Senior Research Scientist at JPL. He has published more than 150 technical papers and reports.

Simon H. Yueh (M'92) received the S.B.and S.M. degrees from the Electrical Engineering Department of the National Taiwan University, Taipei, Taiwan, R.O.C., in 1982 and 1984, respectively, and the Ph.D. degree in electrical engineering from the Massachusetts Institute of Technology (MIT), Cambridge, in 1991. From February to August 1991, he was a Postdoctoral Research Associate at MIT, where he developed various techniques for the calibration of polarimetric radars and theoretical models for the remote sensing of rough surfaces and vegetation.

In 1991, he joined the Radar Science and Engineering section at the Jet Propulsion Laboratory, California Institute of Technology, Pasadena, where he has been working on advanced active and passive microwave techniques for ocean surface remote sensing. He has been the principal investigator and co-investigator of numerous NASA and NPOESS projects on ocean surface research. He has authored four book chapters and published 40 refereed articles. His current fields of interest include techniques and instrument developments for microwave remote sensing of soil moisture, ocean surface salinity, ocean winds, and polar ice and theories for active and passive microwave remote sensing.

Dr. Yueh received the 1995 IEEE GRSS Transaction Prize Paper Award for a paper on polarimetric radiometry. He also received the 1998 JPL Director Lew Allen Award for Excellence in recognition for his pioneering research of passive microwave polarimetric remote sensing to earth surface investigations.

Steven J. Dinardo received the B.S.E.E degree from California State University, Los Angeles in 1983.

In 1978, he joined NASA Jet Propulsion Laboratory (JPL). Pasadena, CA, where he has been involved in various projects, including very long base interferometry (VLBI), mobile VLBI, orbiting VLBI, GPS receiver development, and international GPS service. From 1995 through 1997, he was responsible for the deployment of the JPL aircraft polarimetric wind radiometers on NASA's DC-8 and P-3. He successfully coordinated the Hurricane Ocean Wind Experiment, sponsored by NASA and NPOESS, resulting in the first airborne Ku-Band scatterometers and multifrequecy polarimetric radiometers flights over hurricanes. He has also been responsible for development and deployment of JPL's aircraft rain radar and a 94-GHz cloud profiling radar on NASA's DC-8. He is currently involved in the development of low noise microwave radiometers and radar systems for aircraft and spacecraft for remote sensing of soil moisture and ocean salinity.

Seth L. Chazanoff received the B.S. degree in computer and information sciences from The Ohio State University, Columbus, in 1978 and the M.S. degree in computer science from West Coast University, Los Angeles, CA, in 1989.

He joined the Jet Propulsion Laboratory, Pasadena, CA, in 1978, where he is currently a Senior Engineer.

Amarit Kitiyakara received the B.S.E.E. and M.S.E.E. degrees from Stanford University, Palo Alto, CA in 1990 and 1991, respectively.

He joined the Jet Propulsion Laboratory, Pasadena, CA, in 1993 where he develops microwave systems for Earth remote sensing. Current projects include the JASON-1 Microwave Radiometer (JMR), an atmospheric water vapor sensor for the JASON-1 ocean altimetry mission, and the Wide Swath Ocean Altimeter (WSOA), an experimental radar interferometer for global mapping of mesoscale ocean features.

Fuk K. Li (SM'89–F'96) received the B.Sc. and Ph.D. degrees in physics from the Massachusetts Institute of Technology, Cambridge, in 1975 and 1979, respectively.

He joined the Jet Propulsion Laboratory (JPL), California Institute of Technology, Pasadena, in 1979 and has been involved in various radar remote sensing activities. He has developed a number of system analysis tools for spaceborne synthetic aperture radar (SAR) system design, a digital SAR processor and simulator, investigated techniques for multilook processing and Doppler parameter estimations for spaceborne SARs and evaluated the tradeoffs in SAR image parameters. He also participated in the development of system design concepts and applications for interferometric SAR. He was the Project Engineer for the NASA Scatterometer and was responsible for the technical design of the system. He was the principal investigator for an airborne rain mapping radar and was using data obtained from that system for rain retrieval algorithm development studies in support of the Tropical Rain Measuring Mission. He was also a principal investigator for an experiment utilizing the SIR-C/X-SAR systems to study rainfall effects on ocean roughness and rain retrieval with multiparameter SAR observations from space. He is also leading the development of an airborne cloud profiling radar and the development of an active/passive microwave sensor for ocean salinity and soil mositure sensing. He is currently Manager of the New Millennium Program.

Yahya Rahmat-Samii (S'73–M'75–SM'79–F'85) received the M.S. and Ph.D. degrees in electrical engineering from the University of Illinois, Urbana, in 1971 and 1975, respectively.

Currently, he is a Professor of electrical engineering at the University of California, Los Angeles (UCLA). He was a Senior Research Scientist at NASA's Jet Propulsion Laboratory, California Institute of Technology, before joining UCLA. He was a Guest Professor at the Technical University of Denmark, Lyngby, in the summer of 1986. He has also been a consultant to many aerospace companies. He has authored and coauthored over 450 technical journal articles and conference papers and has written 14 book chapters. He is the coauthor of *Electromagnetic Optimization by Genetic Algorithms* (New York: Wiley, 1999) and *Impedance Boundary Conditions in Electromagnetics* (Washington, DC: Taylor & Francis, 1995). He is also the holder of several patents. He has had pioneering research contributions in diverse areas of electromagnetics, antennas, measurement and diagnostics techniques, numerical and asymptotic methods, satellite and personal communications and human/antenna interactions, etc. (for more information, see http://www.antlab.ee.ucla.edu).

Dr. Rahmat-Samii was the 1995 President and 1994 Vice-President of IEEE Antennas and Propagation Society. He was appointed an IEEE Antennas and Propagation Society Distinguished Lecturer and presented lectures internationally. He was elected a Fellow of IAE in 1986. He was also a member of the Strategic Planning and Review Committee (SPARC) of the IEEE. He has been the guest and plenary session speaker at many national and international symposia. He was one of the directors and Vice President of the Antennas Measurement Techniques Association (AMTA) for three years. He has been Editor and Guest Editor of many technical journals and book publication entities. He has also served as Chairman and Co-Chairman of several national and international symposia. He was also a member of UCLA's graduate council for three years. For his contributions, he has received numerous NASA and JPL Certificates of Recognition. In 1984, he was the recipient of the prestigious Henry Booker Award of URSI. In 1992 and 1995, he was the recipient of the Best Application Paper Award (Wheeler Award) for papers published in the 1991 and 1993 IEEE TRANSACTIONS ON ANTENNAS AND PROPAGATION. In 1993, 1994, and 1995, three of his Ph.D. students were named the Most Outstanding Ph.D. Students at UCLA's School of Engineering and Applied Science. Five others received various student paper awards at the 1993, 1996, 1997, and 1998 IEEE AP-S/URSI symposia. He has recently been selected as one of the recipients of the IEEE Millennium Medals. He is a member of Commissions A, B, and J of USNC/URSI, AMTA, Sigma Xi, Eta Kappa Nu, and the Electromagnetics Academy. He is listed in *Who's Who in America*, *Who's Who in Frontiers of Science and Technology*, and *Who's Who in Engineering.* In 1999, he was the recipient of Distinguished Alumni Award of the University of Illinois. In 2000, he was the recipient of the IEEE Third Millennium Medal and the AMTA Distinguished Achievement Award.